

Off-axis MeV and very-high-energy gamma-ray emissions from structured gamma-ray burst jets

Željka Bošnjak,^{1*} B. Theodore Zhang (张兵)[†],² Kohta Murase[‡],^{3,4,5,6,2} and Kunihito Ioka[§]²

¹Faculty of Electrical Engineering and Computing, University of Zagreb, Unska ul. 3, 10000 Zagreb, Croatia

²Center for Gravitational Physics and Quantum Information, Yukawa Institute for Theoretical Physics, Kyoto University, Kyoto, Kyoto 606-8502, Japan

³Department of Physics, The Pennsylvania State University, University Park, PA 16802, USA

⁴Department of Astronomy & Astrophysics, The Pennsylvania State University, University Park, PA 16802, USA

⁵Center for Multimessenger Astrophysics, Institute for Gravitation and the Cosmos, The Pennsylvania State University, University Park, PA 16802, USA

⁶School of Natural Sciences, Institute for Advanced Study, Princeton, NJ 08540, USA

Accepted XXX. Received YYY; in original form ZZZ

ABSTRACT

Very-high-energy (VHE) photons around TeV energies from a gamma-ray burst (GRB) jet will play an essential role in the multi-messenger era, with a fair fraction of the events being observed off-axis to the jet. We show that different energy photons (MeV and TeV photons in particular) arrive from different emission zones for off-axis observers even if the emission radius is the same. The location of the emission region depends on the jet structure of the surface brightness, and the structures are generally different at different energies, mainly due to the attenuation of VHE photons by electron-positron pair creation. This off-axis zone-shift effect does not justify the usual one-zone approximation and also produces a time-delay of VHE photons comparable to the GRB duration, which is crucial for future VHE observations, such as by the Cherenkov Telescope Array.

Key words: radiation mechanisms: general – relativistic processes – stars: jets – transients: gamma-ray bursts

1 INTRODUCTION

The very-high-energy (VHE; ≥ 0.1 TeV) emission has been observed by Imaging Atmospheric Cherenkov telescopes (IACTs) from several gamma-ray bursts (GRB 180720B, GRB 190114C, GRB 190829A, GRB 201015A, GRB 201216C and GRB 221009A; for a recent review see e.g., [Noda & Parsons \(2022\)](#)). Among these, GRB 190829A and GRB 201015A are classified as low-luminosity (LL) GRBs based on their prompt emission luminosity. For short gamma-ray bursts (sGRBs), the MAGIC collaboration has reported a significance of $\sim 3\sigma$ detection of gamma-rays from sGRB 160821B ([MAGIC Collaboration et al. 2020](#)). The detection of GRBs at the VHE band provided new clues for the understanding of the physics of GRBs, as modeling the emission on a broad energy range from optical to TeV allows us to constrain the microphysics parameters in the emission regions (e.g., [Derishev & Piran 2021](#); [Asano et al. 2020](#)). Even though the origin of VHE gamma-rays from GRBs is consistent with the synchrotron self-Compton (SSC) afterglow model for current observations (e.g., [Meszaros & Rees 1994](#); [Zhang & Meszaros 2001](#); [Sari & Esin 2001](#)), the detection of VHE gamma-rays is expected also during the GRB prompt emission phase (e.g., [Inoue et al. 2013](#); [Vurm & Beloborodov 2017](#); [Bošnjak et al. 2009](#); [Banerjee et al. 2022](#); [Gill & Granot 2022](#)).

The detection of gravitational wave (GW) source GW170817 associated with the short GRB 170817A ([Abbott et al. 2017a,b](#)) opened

a new era in the electromagnetic counterpart search to GRBs ([Lamb & Kobayashi 2017](#); [Ioka & Nakamura 2018](#); [Nakar 2020](#)), as the associated electromagnetic signal potentially allows the identification of the host galaxy and the redshift measurement. The properties of sGRB 170817A were rather uncommon: its γ -ray luminosity ($\sim 10^{47}$ erg/s) was four orders of magnitude lower than typical short GRB, and the prompt emission consisted of two distinct components showing the unexpected spectral evolution. The first pulse was fitted with a cutoff power-law model with a hard low-energy spectrum, and it was followed by the second pulse dominated by a thermal emission ([Pozanenko et al. 2018](#)). The early observations in the optical/near-infrared band were interpreted as quasi-thermal radiation from a kilonova ([Tanaka et al. 2017](#); [Kasen et al. 2017](#); [Utsumi et al. 2017](#); [Pian et al. 2017](#)). The radio and X-ray observations exhibited a gradual rise in the emission. Early-time X-ray and radio observations were consistent with a wide-angle, mildly relativistic ($\Gamma \sim 2$ -3) cocoon emission ([Kasliwal et al. 2017](#)). The VLBI observations of the superluminal motion suggested that the late-time emission was dominated by the narrowly-collimated ($\theta_c \lesssim 5^\circ$) jet, observed from a large viewing angle $\sim 14^\circ$ - 28° ([Mooley et al. 2018b](#); [Ghirlanda et al. 2019](#)). As a viable scenario for the interpretation of the steadily rising afterglow luminosity in radio to X-ray ([Margutti et al. 2018](#); [Mooley et al. 2018a](#)), the structured jet was discussed ([Ioka & Nakamura 2019](#); [Lazzati et al. 2018](#); [Urrutia et al. 2021](#); [Takahashi & Ioka 2021](#)).

The angular structure of the GRB jets was proposed early on (e.g., [Mészáros et al. 1998](#); [Zhang et al. 2004](#); [Rossi & Rees 2003](#); [Kumar & Granot 2003](#); [Granot & Kumar 2003](#)) as it may be arising during the jet launch or during the interaction of the jet with the dense

* E-mail: zeljka.bosnjak@fer.hr(ZB)

† E-mail: bing.zhang@yukawa.kyoto-u.ac.jp (BTZ)

‡ E-mail: murase@psu.edu (KM)

§ E-mail: kunihito.ioka@yukawa.kyoto-u.ac.jp (KI)

environment following the merger of a neutron star binary (Aloy et al. 2005; Murguia-Berthier et al. 2017; Kathirgamaraju et al. 2018; Preau et al. 2021; Gottlieb et al. 2021); for a recent review see Salafia & Ghirlanda (2022).

In this work, we study the emission zone of VHE gamma-rays for a structured jet, similar to GW170817/GRB 170817A when viewed off-axis. We focus on the model described in Ioka & Nakamura (2019), where the off-axis emission arrives largely from the off-center jet when the jet luminosity is decreasing sharply outward as it is required from the observations of GRB 170817A. Matsumoto et al. (2019) revisited the compactness of the gamma-ray sources given by Lithwick & Sari (2001) for arbitrary viewing angles, and confirmed that the relativistic jet core cannot be the origin of the observed emission in GRB 170817A. Future VHE facilities such as CTA will allow the follow-up of the gravitational events in the VHE band, and GW170817-like objects are promising sources of off-axis VHE gamma rays (Murase et al. 2018). We apply these findings in the study of the observed surface brightness of the jet emission taking into account the opacity of the source to gamma-rays. Recently, Hendriks et al. (2022) simulated a population of binary neutron stars observed by GW detectors (LIGO, Virgo, the Einstein Telescope and the Cosmic Explorer) and made predictions for the detection of sGRBs by *Fermi*/GBM, *Swift*/BAT and GECAM using a top-hat jet model for a GRB. Our study can also be implemented in such simulations to make predictions for future VHE observations.

This kind of study can be interesting also for LL GRBs (Soderberg et al. 2006; Liang et al. 2007). For LL GRBs often the relativistic shock breakout model is discussed (Campana et al. 2006; Nakar & Sari 2012; Nakar 2015), where the energy deposition is done by a narrow jet in the low-mass extended material. The induced shock is much less relativistic than the jet, and after the breakout produces the low-luminosity soft gamma-rays which are not narrowly beamed. The off-axis jet model was proposed for the interpretation of GRB emission properties in several events (Ioka & Nakamura 2001; Yamazaki et al. 2003; Waxman 2004; Sato et al. 2021). LL GRBs are promising targets for future VHE facilities due to their predicted high local rate (Wanderman & Piran 2010) and consequently, GeV/TeV observations being less affected by the extragalactic background light (EBL) attenuation (Murase et al. 2008; Rudolph et al. 2022). The asymmetric collapse of massive stars may also be the source of GW emission (Shibata et al. 2021), where the interesting candidates are nearby low-luminosity GRBs (Kobayashi & Mészáros 2003; Daigne & Mochkovitch 2007; Nakar 2015).

This paper is organized as follows: In Sec. 2, we describe the details of the off-axis structured jet model. In Sec. 3, we discuss the origin of VHE gamma-rays and the optical depth due to the two-photon pair annihilation based on a structured jet model. Our main results are presented in Sec. 4, where we arrive at the conclusion that different energy photons arrive from different emission zones in general. In Sec. 5, we discuss the detectability of the time delay. In Sec. 6, we study other effects that may affect our results and discuss the implications of this work. Finally, we give a summary in Sec. 7.

2 STRUCTURED JET MODEL

In Fig. 1, we show a schematic picture of the emission from an off-axis structured jet that we applied: it consists of an energetic and highly relativistic core, with the energy and Lorentz factor sharply decreasing outwards. Following Ioka & Nakamura (2019), we con-

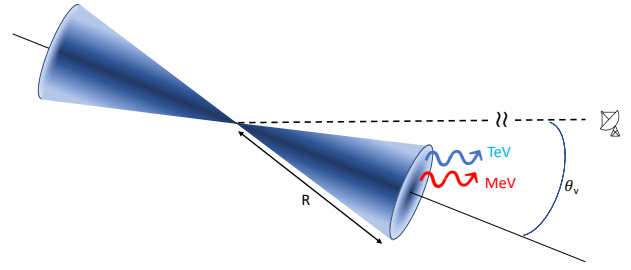


Figure 1. Prompt sub-MeV/MeV and VHE emission from a structured jet with viewing angle θ_v . The distance of the emission region from the center is R when measured in the laboratory frame. We show that different energy photons generally arrive from different emission zones for an off-axis observer.

sider an off-axis structured jet with a Gaussian shape,

$$E_\gamma(\theta) = \epsilon_\gamma E_0 \exp\left(-\frac{\theta^2}{2\theta_c^2}\right), \quad (1)$$

where $E_\gamma(\theta)$ is the isotropic-equivalent radiation energy of the jet at an angle θ from the jet axis, E_0 is the isotropic equivalent energy measured along the jet axis, ϵ_γ is the radiation efficiency, and θ_c is the jet core opening angle (or the standard deviation of the Gaussian distribution). The angle between the line of sight and a direction (θ, ϕ) in the jet can be estimated as

$$\cos\theta_\Delta = \sin\theta \cos\phi \sin\theta_v + \cos\theta \cos\theta_v, \quad (2)$$

where θ_v is the viewing angle and ϕ is the azimuth angle with respect to the jet axis. In the following studies, we adopt fiducial values of $E_0 = 10^{52.8}$ erg, $\theta_c = 0.059$ and $\theta_v = 0.38 \approx 22^\circ$ as inferred from the observations of sGRB 170817A (Troja et al. 2019). We assume the radiation efficiency for sub-MeV/MeV prompt emissions is $\epsilon_\gamma = 0.1$ for simplicity. In reality, the radiation efficiency should have an angular structure $\epsilon_\gamma(\theta)$ which depends on the details of the radiative processes. In addition, we assume the Lorentz factor decreases outward with the shape described by the following relation,

$$\Gamma(\theta) = \Gamma_{\max} \frac{1}{1 + (\theta/\theta_c)^\lambda}, \quad (3)$$

where $\Gamma_{\max} = 2000$ and $\lambda = 3.8$ (Ioka & Nakamura 2019). We assume the energy of the structured jet dissipated at a distance R from the explosion center in the laboratory frame, where the emission region could be described by a relativistic shocked shell with comoving width $\Delta' \sim R/\Gamma(\theta)$. The corresponding timescales could be estimated as $\sim R/\Gamma(\theta)^2 c$. However, the energy dissipation radius is difficult to predict without the knowledge of the jet composition and radial profile. In this work, we consider the energy dissipation that occurred at the fixed radius R , and we will show that different energy photons generally arrive from different portions even for the same radius.

3 VHE PROMPT EMISSION AND OPTICAL DEPTH

In recent years, several GRBs have been observed at the VHE band, including both, high and low luminosity GRBs. All of the present VHE observations are consistent with the origin at the afterglow phase. The unequivocal VHE emission during the prompt phase has

not been detected yet, though it is possible that in the early VHE observations by MAGIC telescopes of GRB 190114C there was a contribution by the late prompt emission (MAGIC Collaboration et al. 2019). One of the difficulties faced when observing prompt emission is the duration of the response time following the alert system for IACTs.

In this work, we consider the detection of VHE emission during the prompt phase. For the synchrotron emission from high-energy electrons, the maximum photon energy is $\sim 50\Gamma/(1+z)$ MeV due to the limitation of the synchrotron energy loss process. The maximum photon energy could be somewhat increased considering the situation where high-energy electrons are accelerated far from the shock front where the magnetic field strength is lower but emit efficiently when these electrons travel near the shock front where the magnetic field strength is larger (Kumar et al. 2012). The inverse-Compton (IC) process would be more reliable to generate high-energy photons via upscattering low-energy photons to higher energies. The synchrotron self-Compton (SSC) process, where the same population of the non-thermal electrons produces synchrotron emission could also upscatter these photons to higher energies, and has been successful in explaining the observed VHE emission in the afterglow phase. However, the SSC process may not be efficient in the prompt phase due to the Klein-Nishina effect, where the IC cross-section for scattering decreases significantly. It occurs for the photon energies comparable to the electron rest mass when measured in the electron rest frame, $\gamma_e v'_b \sim m_e c^2$, where v'_b is the target photon energy measured in the comoving frame. Nevertheless, if there are external photons, i.e., external thermal or non-thermal photons that overwhelm the prompt Band component in the low-energy range, the external inverse-Compton (EIC) process will dominate the high-energy photons at the VHE band. The origin of thermal photons could come from stellar emission or cocoon emission (e.g., Toma et al. 2009; De Colle et al. 2018; Kimura et al. 2019) and internal dissipation such as flares and extended emission (e.g., Murase et al. 2018). The VHE gamma-rays in the prompt phase could also be contributed by the hadronic processes (Asano & Inoue 2007; Gupta & Zhang 2007; Razzaque et al. 2009; Murase et al. 2012; Rudolph et al. 2023).

The low-energy (LE) sub-MeV/MeV prompt emission could be modeled with a spectral shape similar to the so-called Band function (e.g., Ioka & Nakamura 2019),

$$f(v', \theta) = \frac{C}{v'_0(\theta)} \left(\frac{v'}{v'_0(\theta)} \right)^{1+\alpha_B} \left[1 + \left(\frac{v'}{v'_0(\theta)} \right)^2 \right]^{\frac{\beta_B - \alpha_B}{2}}, \quad (4)$$

where the constant C is chosen so that $\int dv' f(v', \theta) = 1$. We adopt the following relation for the observed peak energy $\nu_{0,\text{LE}}(\theta, \phi)$ based on the observations of sGRB 170817A and the requirement to satisfy the Amati relation,

$$\nu_{0,\text{LE}}(\theta, \phi) = \delta_D \nu'_{0,\text{LE}}(\theta) \approx 0.15 \times 10^3 \delta_D \left[1 + \left(\frac{\theta}{\theta_c} \right)^{3.4} \right] \text{eV}, \quad (5)$$

where $\delta_D = 1/(\Gamma(1 - \beta \cos \theta_\Delta))$ is the Doppler factor, and $\nu'_{0,\text{LE}}(\theta)$ is the peak energy in the comoving frame.

To model the energy spectrum at the VHE band of the prompt emission, we adopt a toy model which shares similar spectral properties as the low-energy prompt emission, with HE spectral peak

$$\nu_{0,\text{VHE}}(\theta, \phi) = \delta_D \nu'_{0,\text{HE}}(\theta) \approx 0.15 \times 10^9 \delta_D \left[1 + \left(\frac{\theta}{\theta_c} \right)^{3.4} \right] \text{eV}, \quad (6)$$

where $\nu_{0,\text{HE}}(\theta, \phi)$ is the observed peak energy of the VHE prompt emission.

The optical depth for the two-photon pair annihilation process can be estimated as (e.g., Murase et al. 2016),

$$\begin{aligned} \tau_{\gamma\gamma}(v, \theta, \phi) &\approx n'(\tilde{\nu}') l' \sigma_{\gamma\gamma} \\ &\approx \frac{1}{4\pi R^2 \Delta R' \tilde{\nu}'} \frac{E_\gamma(\theta)}{\Gamma(\theta)} f(\tilde{\nu}', \theta) l' \sigma_{\gamma\gamma} \\ &\approx 1.6 \left(\frac{R}{10^{14} \text{ cm}} \right)^{-2} \frac{\zeta(\theta)}{\zeta(4.5\theta_c)}, \end{aligned} \quad (7)$$

where

$$\zeta(\theta) = (E_\gamma(\theta)/\Gamma(\theta))(f(\tilde{\nu}', \theta)/\tilde{\nu}'). \quad (8)$$

Also, $n'(\tilde{\nu}')$ is the comoving frame target photon number density at the characteristic energy $\tilde{\nu}' \approx \delta_D (m_e c^2)^2 / \nu$, R is the distance of the emission region that is measured in the lab frame, $\Delta R' \sim R/\Gamma(\theta)$ is the comoving shell width and the thickness of the gamma-ray emission region, $E_\gamma(\theta)/\Gamma(\theta)$ is the comoving radiation energy, l' is the photon path length before escaping from the source, and $\sigma_{\gamma\gamma} \sim (7/12)\sigma_T$ is the cross section (e.g., Svensson 1987). We simply assume $l' \sim \Delta R'$ (Matsumoto et al. 2019). In the above estimates, we assume a broken power-law distribution with $\alpha_B = -1$ and $\beta_B = -2.5$. We can see the optical depth depends on the distance of the emission region with $\tau_{\gamma\gamma} \propto R^{-2}$. The optical depth also depends on the polar angle, where $\zeta(\theta)$ sharply decreases with increasing θ when $\theta \gtrsim 2\theta_c$. In the above estimates, we assume $\theta = 4.5\theta_c = 0.26 \approx 15^\circ$ and $\nu = 1$ TeV. Note that we do not consider here the contribution to optical depth from scatterings of photons by e^\pm created by the annihilation of photon pairs, as in case when this contribution was large we would expect the burst to be optically thick to all photons, independently on their energy (Lithwick & Sari 2001).

The mean escape probability, or the attenuation factor, of the VHE emission, can be derived by solving the radiative transfer equation assuming uniform slab geometry (Svensson 1987),

$$\xi(v, \theta, \phi) = \frac{1 - e^{-\tau_{\gamma\gamma}(v, \theta, \phi)}}{\tau_{\gamma\gamma}(v, \theta, \phi)}, \quad (9)$$

which is $\xi \approx 0.6$ for $\tau_{\gamma\gamma} = 1$ and $\xi \approx 0.1$ for $\tau_{\gamma\gamma} = 10$. In general, the optical depth $\tau_{\gamma\gamma}$ at a certain radius depends on the initial assumptions on Lorentz factor and energy profile, and on the Doppler factor.

4 DIFFERENT ENERGY PHOTONS FROM DIFFERENT EMISSION ZONES

The specific surface brightness per solid angle per frequency can be expressed as (Ioka & Nakamura 2018)

$$\frac{dE_{\gamma,\text{iso}}}{d\Omega dv} = \frac{1}{4\pi} \frac{E_\gamma(\theta) [f(v, \theta, \phi; \nu_{0,\text{LE}}) + f_{\text{HE}}(v, \theta, \phi; \nu_{0,\text{HE}})] \xi(v, \theta, \phi)}{\Gamma(\theta)^4 [1 - \beta(\theta) \cos \theta_\Delta]^3}, \quad (10)$$

where $\int dv f(v, \theta, \phi; \nu_{0,\text{LE}}) = 1$ and $\int dv f_{\text{HE}}(v, \theta, \phi; \nu_{0,\text{HE}}) = 1/5$, and we assume the total energy radiated in the VHE energy band takes only $\sim 20\%$ of the total energy radiated in the low-energy sub-MeV/MeV band (this assumption would slightly increase the adopted value for radiative efficiency ϵ_γ). Here $f_{\text{HE}}(v, \theta, \phi; \nu_{0,\text{HE}})$ has the same form as the low-energy spectrum given by Eq. 4, with the spectral peak in the comoving frame as in Eq. 6.

In Figs. 2 and 3, we show the surface brightness distribution,

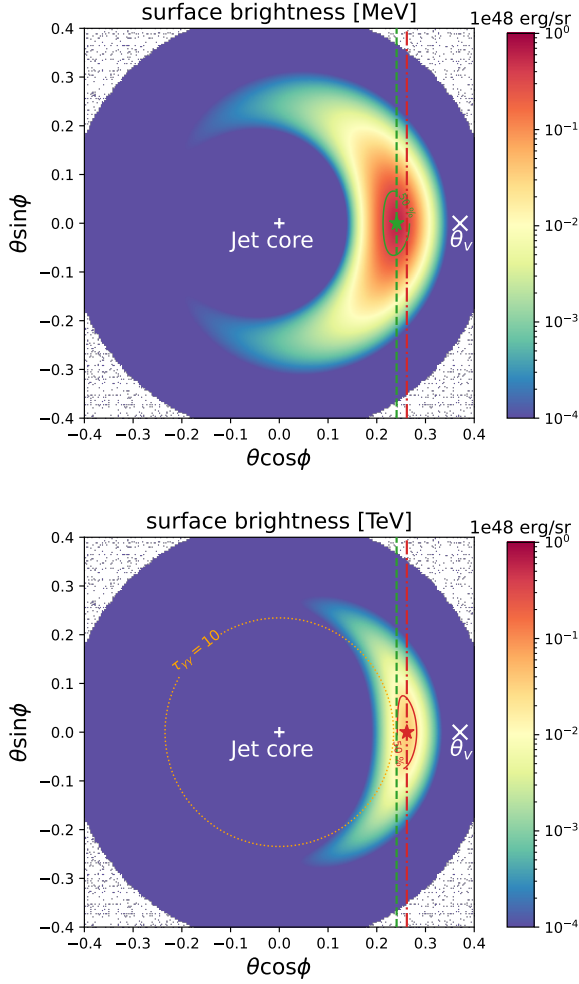


Figure 2. The surface brightness distribution at the MeV band (upper panel) and TeV band (lower panel) of a structured jet for $\Gamma_{\max} = 2000$ and $R = 10^{14}$ cm. The position of the jet core is indicated as a white plus symbol and the viewing angle θ_v is marked as a white cross symbol. We can see that the emission regions with 50% surface brightness are shifted between the MeV and TeV bands (see also Fig. 4). This is mainly caused by the high optical depth of TeV gamma-rays ($\tau_{\gamma\gamma} = 10$ line with orange dotted line). The different emission region also leads to different arrival time in Fig. 5.

$vdE_{\gamma,\text{iso}}/d\Omega dv$, on the jet surface at the MeV and TeV bands, respectively. The peak position of the specific surface brightness is indicated by a green star at the MeV band (upper panel) and a red star at the TeV band (lower panel). Due to the effect of the Doppler boost, the observed brightness for the off-axis structured jet is dominated by a small patch centered on the peak position with typical angular size $\Delta\Omega$,

$$\frac{dE_{\nu,\text{iso}}}{d\nu} \approx \frac{dE_{\nu,\text{iso}}}{d\Omega d\nu} \Delta\Omega, \quad (11)$$

where $\Delta\Omega$ could be approximated as the region surrounded by the solid contours, which represents the position where the surface brightness decreases by a factor of 50% compared to the peak value. The dotted circle in the lower panels is the position where the optical depth for TeV photons equals $\tau_{\gamma\gamma} = 10$. While the peak position of the surface brightness is shifted at the TeV band with respect to MeV band for smaller radius ($R = 10^{14}$ cm, see Fig. 2), this shift becomes

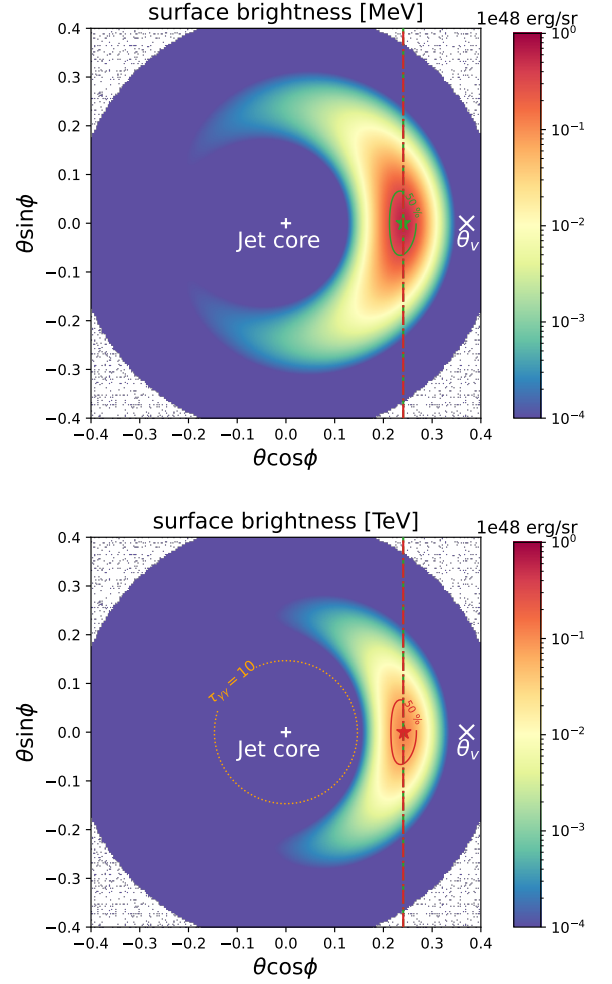


Figure 3. Same as Fig. 2, but for $R = 10^{15}$ cm. The shift of the peak position of the specific surface brightness between the MeV and TeV bands becomes much smaller.

much smaller at higher radii, see e.g. Fig. 3 for $R = 10^{15}$ cm. However, the region where the surface brightness decreased by a factor of 50% becomes apparently larger, indicating the larger time spread of the arrival times for the TeV emission (this effect adds up to the difference in photon arrival times due to the different emission radii, see Fig. 5). Note that we did not include the evolution of different parameters (e.g. Lorentz factor, spectral properties) with radius in our calculation, while this may be expected with the jet propagation.

In conclusion, we could expect different energy photons to come from different emission zones for a structured jet when viewed off-axis. This is because the surface brightness distribution is different at different frequencies, mainly due to the different optical depth with more attenuation at the TeV band than the MeV band (and partly due to the different segment of the observed spectrum).

An important implication is that a popular one-zone approximation in the spectral analysis is not justified at all in the off-axis jet case. With the current facilities it is impossible to resolve the emission region for GRBs. One of the observable effects of such a phenomenon is the arrival time of photons from different emission regions, which we will discuss in the following section.

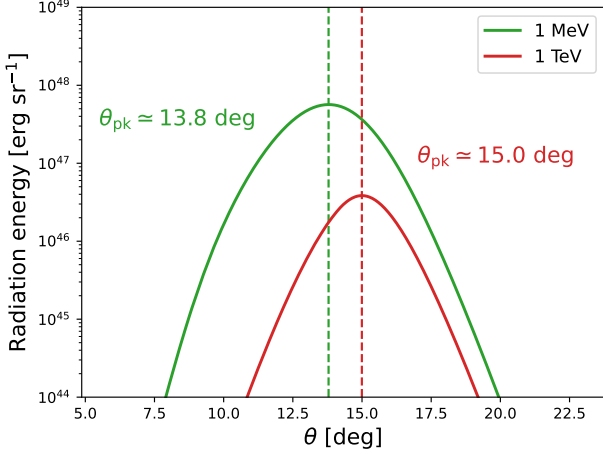


Figure 4. Similar to Fig. 2, we show the surface brightness distribution as a function of the polar angle θ when $\phi = 0$.

5 PHOTON ARRIVAL TIME AND POSSIBLE TIME DELAY

For a relativistic structured jet, photons emitted at the same lab frame time t at different locations may arrive at the observer at the same observed time T (e.g., Zhang 2018). The observed time T is related to the time in the laboratory frame t as

$$T = t - \frac{R}{c} \cos \theta_{\Delta}, \quad (12)$$

where R is the radius of the emitting shell measured in the laboratory frame. The laboratory frame time t can be estimated as

$$t = \int_0^R \frac{dr}{\beta(\theta)c} \approx \frac{R}{\beta(\theta)c}. \quad (13)$$

The above approximation in Eq. 13 is valid if there is no acceleration or deceleration of the relativistic shell during the propagation. The observed time T is

$$T = \frac{R}{c\beta(\theta)} (1 - \beta(\theta)\cos\theta_{\Delta}) \approx \begin{cases} \frac{R}{2c\Gamma(\theta)^2} & (\theta_{\Delta} < 1/\Gamma(\theta)) \\ \frac{R\theta_{\Delta}^2}{2c} & (\theta_{\Delta} > 1/\Gamma(\theta)) \end{cases}, \quad (14)$$

where $\beta(\theta) \approx 1 - 1/2\Gamma^2$ and $\cos \theta_{\Delta} \approx 1 - \theta_{\Delta}^2/2$. From Eq. 14, we can see that the observed time T reaches a minimum value when $\theta_{\Delta} \sim 1/\Gamma$.

As shown in Fig. 4, the peak position of the surface brightness along the direction of $\phi = 0$ is $\theta_{\text{MeV}} \approx 13.8$ deg at the MeV energy band and $\theta_{\text{TeV}} \approx 15.0$ deg at the TeV energy band, respectively. The relative difference in the arrival time of TeV and MeV photons is shown in Fig. 5 as a function of the emission radius. Our results indicate that the arrival of the TeV photons is typically delayed compared to MeV photons, and the value reaches a maximum of approximately $T_{\text{pk, delay}} \sim 8$ s when $R = 10^{13.75}$ cm, see the purple thick solid curve in Fig. 5.

The time delay between the TeV photons and MeV photons is caused by the fact that the TeV photons and MeV photons have different surface brightness, mainly due to the two-photon annihilation optical depth, see Fig. 2. The reason is that the emission zone of MeV photons is typically located at $\theta_{\text{MeV}} \sim \theta_{\text{min}}$, where T reaches

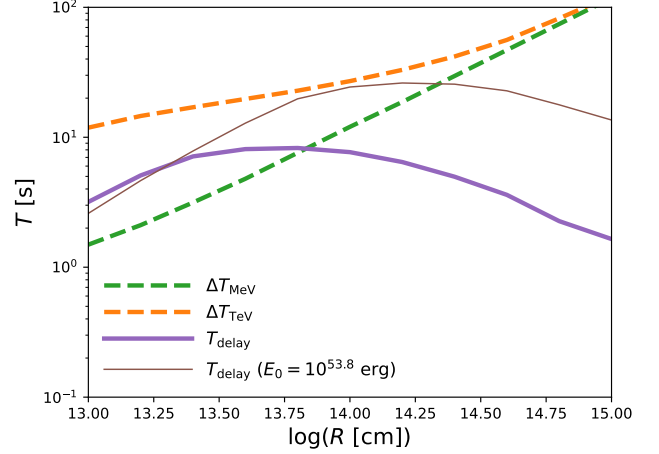


Figure 5. The arrival time delay between TeV and MeV photons and the duration of GRB prompt emission at the MeV energy band as a function of the emission region radius. The spectral and jet parameters are the same as in Fig. 2. Note that the viewing angle is set to $\theta_v = 0.38$.

a minimum at θ_{min} . However, the emission zone of TeV photons is located at $\theta_{\text{TeV}} > \theta_{\text{min}}$, where T is larger. At a smaller radius, the whole VHE emission region is significantly attenuated due to the larger optical depth. With the increase of the emission radius, the VHE emission region near the center is still optical thick, but the outer region becomes transparent. Under such a situation, only VHE photons from the outer region could escape which are delayed compared to MeV photons. The time delay between TeV and MeV photons becomes smaller for larger radius, i.e. $R \gtrsim 10^{15}$ cm, where both the VHE emission region and sub-MeV/MeV emission region are optically thin.

We also show the time spread of the arrival times (duration) of the MeV prompt emission from the interior of the half-maximum surface brightness line as a function of radius in dashed green line. Similarly, the duration of the TeV emission is shown in dashed orange line. We can see that it is possible that the time delay between TeV and MeV photons could be larger than the typical duration of the MeV prompt emission. The typical time delay between TeV and MeV photons could be significant for energetic events when $E_0 = 10^{53.8}$ erg because the VHE emission region move outwards due to the higher optical depth of TeV gamma-rays, see the brown thin solid curve.

With the current and near-future VHE gamma-ray facilities, especially with the operation of CTA (The CTA Consortium 2019), one may expect co-incident detections of nearby GRBs at the VHE band with gravitational waves (e.g., Murase et al. 2018; Bartos et al. 2019). The study in this work suggests that the TeV emission pulse could lag behind the main pulse of the prompt emission at the MeV band, which could compensate for the large slewing time of CTA, which is $t_{\text{slew}} \sim 20$ s for CTA-LST and $t_{\text{slew}} \sim 90$ s for CTA-MST (Banerjee et al. 2022). This effect, therefore, increases the probability of observing the TeV emission from short gamma-ray bursts during the prompt phase by CTA. Also, the possibility of the prolonged duration of the prompt phase may be interesting for interpreting the observed features of long GRBs linked to the compact object binary mergers, e.g. GRB 211211A (Troja et al. 2022; Yang et al. 2022; Mei et al. 2022; Rastinejad et al. 2022).

6 DISCUSSION AND IMPLICATIONS

When considering the off-axis structured jets, we found that different energy photons could arrive from different emission zones mainly due to the effect of the two-photon pair annihilation process. The main reason is that the optical depth for VHE photons is much higher in the core region on the jet surface, which gradually decreases outwards allowing VHE photons to escape. In addition, we showed that the optical depth for VHE photons is sensitive to the emission radius, where the corresponding time delay between the typical arrival time of the TeV and MeV emission decreases with the increase of the emission radius. Such a phenomenon could be prominent if the optical depth sharply decreases across the emission zone, such as in the case of the Gaussian jet adopted in this work, where $\zeta(\theta)$ strongly depends on $E_\gamma(\theta)$. A similar effect is possible for the power-law structure of the jet energy if the power-law index is steep. Note that the angular dependence of the optical depth on the Lorentz factor $\Gamma(\theta)$ and energy spectrum $\nu'_{0,\text{HE}}(\theta)$ could also significantly affect the surface brightness distribution for different energy photons. The delayed arrival of \geq TeV photons is also expected in the EIC model (e.g., Murase et al. 2010; Kimura et al. 2019; Zhang et al. 2023), without considering the structured jet.

Another important factor is the viewing angle θ_v . If θ_v is close to or smaller than the jet core, we cannot resolve different emission regions which are similar to the on-axis case. However, if θ_v is too large, the received flux would be lower than the detection threshold. The gravitational-wave data could provide an independent measurement of the inclination angle between the direction of the line-of-sight and jet axis (Biscoveanu et al. 2020). At present, we can only say that for an off-axis structured jet with properties similar to sGRB 170817A, different energy photons could originate from different emission zones. Banerjee et al. (2022) estimated the minimum isotropic energy $\sim 10^{47}$ ergs required for the detection of an event at $z \sim 0.1$ (up to which the current GW detectors are expected to observe BNS mergers), and that would allow for this effect to be observed by the CTA.

7 SUMMARY

The off-axis model for the short gamma-ray burst GRB 170817A predicted that the most luminous region arises neither from the jet core around the primary axis, nor at the line of sight at the viewing angle θ_v , but from the off-centre jet (Ioka & Nakamura 2019). Adopting the same assumptions in this study, we showed that different energy photons could arrive to the observer from different emission zones for off-axis structured jets, and that the typical arrival time of VHE photons could be delayed compared to the typical arrival time of prompt sub-MeV/MeV photons. We discussed how the change in the emission radius could affect the VHE emission region and related arrival times. Our results depend on the angular evolution of the total radiation energy E_γ and of the Lorentz factor, and on the energy spectrum (currently the spectral evolution with radius was not accounted for). The off-axis structured jet could also be observed with a smaller or larger viewing angle depending on the energetics and detector threshold. One of the predictions of our model is the difference between the observed arrival time of prompt MeV emission and high-energy TeV emission. In general, the observation of the time arrival difference brings information on the emission radius.

This model could be applicable to nearby short GRBs, VHE afterglow emission for energetic bursts, but also to LL GRBs, which are interesting as possible TeV emission and neutrino/UHECR sources

(Murase et al. 2008; Murase & Beacom 2010; Boncioli et al. 2019; Rudolph et al. 2022). As LL GRBs have presumably lower ejecta velocities and larger opening angles (Bromberg et al. 2011; Cano et al. 2017; Rudolph et al. 2022), the different assumptions should be taken into account for the estimates of the emission zones for MeV/TeV photons.

ACKNOWLEDGEMENTS

Ž.B. acknowledges the support by FY2022 JSPS Invitational Fellowship for Research in Japan (Short-term) S22013. This work is partly supported by KAKENHI No. 23H05430, 23H04900, 22H00130, 20h01901, 20H01904, 20H00158 (K.I.). The work of K.M. is supported by the NSF Grant No. AST-1908689, No. AST-2108466 and No. AST-2108467, and KAKENHI No. 20H01901 and No. 20H05852.

DATA AVAILABILITY

The data developed for the calculation in this work is available upon request.

REFERENCES

- Abbott B. P., et al., 2017a, *Phys. Rev. Lett.*, **119**, 161101
 Abbott B. P., et al., 2017b, *ApJ*, **848**, L13
 Aloy M. A., Janka H. T., Müller E., 2005, *A&A*, **436**, 273
 Asano K., Inoue S., 2007, *The Astrophysical Journal*, **671**, 645
 Asano K., Murase K., Toma K., 2020, *ApJ*, **905**, 105
 Banerjee B., et al., 2022, *arXiv e-prints*, p. arXiv:2212.14007
 Bartos I., Corley K. R., Gupte N., Ash N., Márka Z., Márka S., 2019, *Mon. Not. Roy. Astron. Soc.*, **490**, 3476
 Biscoveanu S., Thrane E., Vitale S., 2020, *ApJ*, **893**, 38
 Boncioli D., Biehl D., Winter W., 2019, *ApJ*, **872**, 110
 Bošnjak Ž., Daigne F., Dubus G., 2009, *A&A*, **498**, 677
 Bromberg O., Nakar E., Piran T., 2011, *ApJ*, **739**, L55
 Campana S., et al., 2006, *Nature*, **442**, 1008
 Cano Z., Wang S.-Q., Dai Z.-G., Wu X.-F., 2017, *Advances in Astronomy*, **2017**, 8929054
 Daigne F., Mochkovitch R., 2007, *A&A*, **465**, 1
 De Colle F., Lu W., Kumar P., Ramirez-Ruiz E., Smoot G., 2018, *MNRAS*, **478**, 4553
 Derishev E., Piran T., 2021, *ApJ*, **923**, 135
 Ghirlanda G., et al., 2019, *Science*, **363**, 968
 Gill R., Granot J., 2022, *Galaxies*, **10**, 74
 Gottlieb O., Nakar E., Bromberg O., 2021, *MNRAS*, **500**, 3511
 Granot J., Kumar P., 2003, *ApJ*, **591**, 1086
 Gupta N., Zhang B., 2007, *Monthly Notices of the Royal Astronomical Society*, **380**, 78
 Hendriks K., Yi S.-X., Nelemans G., 2022, *arXiv e-prints*, p. arXiv:2208.14156
 Inoue S., et al., 2013, *Astroparticle Physics*, **43**, 252
 Ioka K., Nakamura T., 2001, *ApJ*, **554**, L163
 Ioka K., Nakamura T., 2018, *Progress of Theoretical and Experimental Physics*, **2018**, 043E02
 Ioka K., Nakamura T., 2019, *Monthly Notices of the Royal Astronomical Society*, **487**, 4884
 Kasen D., Metzger B., Barnes J., Quataert E., Ramirez-Ruiz E., 2017, *Nature*, **551**, 80
 Kasliwal M. M., et al., 2017, *Science*, **358**, 1559
 Kathirgamaraju A., Barniol Duran R., Giannios D., 2018, *MNRAS*, **473**, L121

- Kimura S. S., Murase K., Ioka K., Kisaka S., Fang K., Mészáros P., 2019, *ApJ*, 887, L16
- Kobayashi S., Mészáros P., 2003, *ApJ*, 589, 861
- Kumar P., Granot J., 2003, *ApJ*, 591, 1075
- Kumar P., Hernández R. A., Bošnjak Ž., Duran R. B., 2012, *Monthly Notices of the Royal Astronomical Society: Letters*, pp no–no
- Lamb G. P., Kobayashi S., 2017, *MNRAS*, 472, 4953
- Lazzati D., Perna R., Morsony B. J., Lopez-Camara D., Cantiello M., Ciolfi R., Giacomazzo B., Workman J. C., 2018, *Phys. Rev. Lett.*, 120, 241103
- Liang E., Zhang B., Virgili F., Dai Z. G., 2007, *ApJ*, 662, 1111
- Lithwick Y., Sari R., 2001, *ApJ*, 555, 540
- MAGIC Collaboration et al., 2019, *Nature*, 575, 459
- MAGIC Collaboration et al., 2020, MAGIC Observations of the Nearby Short Gamma-Ray Burst GRB 160821B ([arXiv:2012.07193](https://arxiv.org/abs/2012.07193)), [doi:10.3847/1538-4357/abd249](https://doi.org/10.3847/1538-4357/abd249)
- Margutti R., et al., 2018, *ApJ*, 856, L18
- Matsumoto T., Nakar E., Piran T., 2019, *MNRAS*, 486, 1563
- Mei A., et al., 2022, *Nature*, 612, 236
- Meszáros P., Rees M. J., 1994, *Monthly Notices of the Royal Astronomical Society*, 269, L41
- Mészáros P., Rees M. J., Wijers R. A. M. J., 1998, *ApJ*, 499, 301
- Mooley K. P., et al., 2018a, *Nature*, 554, 207
- Mooley K. P., et al., 2018b, *Nature*, 561, 355
- Murase K., Beacom J. F., 2010, *Phys. Rev. D*, 82, 043008
- Murase K., Ioka K., Nagataki S., Nakamura T., 2008, *Phys. Rev. D*, 78, 023005
- Murase K., Toma K., Yamazaki R., Nagataki S., Ioka K., 2010, *MNRAS*, 402, L54
- Murase K., Asano K., Terasawa T., Mészáros P., 2012, *ApJ*, 746, 164
- Murase K., Guetta D., Ahlers M., 2016, *Phys. Rev. Lett.*, 116, 071101
- Murase K., et al., 2018, *ApJ*, 854, 60
- Murguía-Berthier A., et al., 2017, *ApJ*, 835, L34
- Nakar E., 2015, *ApJ*, 807, 172
- Nakar E., 2020, *Phys. Rep.*, 886, 1
- Nakar E., Sari R., 2012, *ApJ*, 747, 88
- Noda K., Parsons R. D., 2022, *Galaxies*, 10, 7
- Pian E., et al., 2017, *Nature*, 551, 67
- Pozanenko A. S., et al., 2018, *ApJ*, 852, L30
- Preau E., Ioka K., Mészáros P., 2021, *MNRAS*, 503, 2499
- Rastinejad J. C., et al., 2022, *Nature*, 612, 223
- Razzaque S., Mena O., Dermer C. D., 2009, *ApJ*, 691, L37
- Rossi E., Rees M. J., 2003, *MNRAS*, 339, 881
- Rudolph A., Bošnjak Ž., Palladino A., Sadeh I., Winter W., 2022, *MNRAS*, 511, 5823
- Rudolph A., Petropoulou M., Bošnjak Ž., Winter W., 2023, *ApJ*, 950, 28
- Salafia O. S., Ghirlanda G., 2022, *Galaxies*, 10, 93
- Sari R., Esin A. A., 2001, *ApJ*, 548, 787
- Sato Y., Obayashi K., Yamazaki R., Murase K., Ohira Y., 2021, *MNRAS*, 504, 5647
- Shibata M., Kiuchi K., Fujibayashi S., Sekiguchi Y., 2021, *Phys. Rev. D*, 103, 063037
- Soderberg A. M., et al., 2006, *Nature*, 442, 1014
- Svensson R., 1987, *MNRAS*, 227, 403
- Takahashi K., Ioka K., 2021, *MNRAS*, 501, 5746
- Tanaka M., et al., 2017, *PASJ*, 69, 102
- The CTA Consortium 2019, Science with the Cherenkov Telescope Array. WORLD SCIENTIFIC, [doi:10.1142/10986](https://doi.org/10.1142/10986)
- Toma K., Wu X.-F., Mészáros P., 2009, *ApJ*, 707, 1404
- Troja E., et al., 2019, *Monthly Notices of the Royal Astronomical Society*, p. stz2248
- Troja E., et al., 2022, *Nature*, 612, 228
- Urrutia G., De Colle F., Murguía-Berthier A., Ramirez-Ruiz E., 2021, *MNRAS*, 503, 4363
- Utsumi Y., et al., 2017, *PASJ*, 69, 101
- Vurm I., Beloborodov A. M., 2017, *ApJ*, 846, 152
- Wanderman D., Piran T., 2010, *MNRAS*, 406, 1944
- Waxman E., 2004, *ApJ*, 602, 886
- Yamazaki R., Yonetoku D., Nakamura T., 2003, *ApJ*, 594, L79
- Yang J., et al., 2022, *Nature*, 612, 232
- Zhang B., 2018, The Physics of Gamma-Ray Bursts, [doi:10.1017/9781139226530](https://doi.org/10.1017/9781139226530).
- Zhang B., Meszaros P., 2001, *The Astrophysical Journal*, 559, 110
- Zhang B., Dai X., Lloyd-Ronning N. M., Mészáros P., 2004, *ApJ*, 601, L119
- Zhang B. T., Murase K., Ioka K., Song D., Yuan C., Mészáros P., 2023, *ApJ*, 947, L14

This paper has been typeset from a $\text{\TeX}/\text{\LaTeX}$ file prepared by the author.